Chemical Geology 585 (2021) 120565

Contents lists available at ScienceDirect

Chemical Geology

journal homepage: www.elsevier.com/locate/chemgeo

Magnesium isotope fractionation during alkaline brine evaporation and implications for Precambrian seawater chemistry

Pan Zhang [a], Kang-Jun Huang [a,*], Chongguang Luo [b,*], Heng Chen [c], Zhian Bao [a], Hanjie Wen [b], Xingliang Zhang [a]

[a] State Key Laboratory of Continental Dynamics and Shaanxi Key Laboratory of Early Life and Environment, Department of Geology, Northwest University, Xi'an 710069, China
[b] State Key Laboratory of Ore Deposit Geochemistry, Institute of Geochemistry, Chinese Academy of Sciences, Guiyang 550081, China
[c] Lamont-Doherty Earth Observatory, Columbia University, Palisades, NY 10964, USA

ARTICLE INFO

Editor: Michael E. Boettcher

Keywords:
Magnesium isotopes
Soda ocean hypothesis
Evaporites
Bloedite
Qinghai Lake

ABSTRACT

The chemical evolution of the ocean is one major component of the puzzle of how climate and life have co-evolved over the Earth's history. A "soda ocean" with high alkalinity, high pH, and low calcium concentration in Precambrian has been proposed to explain the emergence and evolution of early life. However, this hypothesis has not been widely accepted due to the lack of reliable tracers for the chemical composition of Precambrian seawater. Evaporite is formed during seawater/brine evaporation and thus has been widely used to reconstruct the ancient seawater/brine chemical composition. Here, evaporation experiments were conducted using Qinghai Lake (QHL) water, a modern soda lake, to provide an analogy of the Precambrian "soda ocean" evaporation and investigate the mineralogical and Mg isotopic signatures of alkaline brine-derived evaporites. Our results show that the evaporation path of QHL water overall covers the stages of hydrous Mg carbonates (hydromagnesite), halite, and bloedite [$Na_2Mg(SO_4)_2{\cdot}4H_2O$] precipitation. The precipitation of hydrous Mg carbonates and bloedite is distinct from the modern seawater evaporation and is accompanied by the removal of up to 85% Mg from brine. The brine gradually becomes enriched in heavy Mg isotopes during evaporation due to the preferential incorporation of light Mg isotopes into precipitates. The fractionation of Mg isotopes is dominantly controlled by the bond structure during hydrous Mg carbonates and bloedite precipitation, and the latter is also slightly influenced by the kinetics in the highly concentrated brine. The Mg isotope fractionation during bloedite dissolution is limited due to the rapid congruent dissolution. The significant Mg isotopic fractionation observed within the hydrous Mg carbonates precipitation during the earliest QHL water evaporation indicates the potential Rayleigh distillation of Mg by alkalinity in the "soda ocean", which is absent in the Phanerozoic oceans. Therefore, the large Mg isotope fractionation during alkaline brine evaporation can be applied to test the existence of Precambrian "soda oceans".

1. Introduction

The presence of liquid water and the existence of life on the Earth for the vast duration of Earth's history implies the Earth has maintained habitable conditions for life (Kasting and Catling, 2003). Since the chemistry of the ocean has changed significantly through Earth history (e.g., Hardie, 1996), understandings on the chemical evolution of the ocean provide a hint to reconstruct the story of how Earth's environment and life co-evolved through time. For example, two long-term cycles in the major ion chemistry of seawater, particularly the Mg/Ca ratio, coincide with the carbonate mineralogy of hypercalcifying organisms and greenhouse-icehouse climates during the Phanerozoic (Stanley and Hardie, 1998). However, the seawater chemistry during the Precambrian era, the most critical period for early life and surface environment evolution, is still enigmatic (Hardie, 1996; Lyons et al., 2014).

The "soda ocean" hypothesis (SOH) postulated that the Precambrian oceans had high carbonate alkalinity (ALK $\approx HCO_3^- + 2{\cdot}CO_3^{2-}$) and low calcium concentration ($Ca^{2+} < HCO_3^-$) that distinguished from the Phanerozoic seawater ($Ca^{2+} > HCO_3^-$), while more resemble present-day soda lakes (Kempe and Degens, 1985). Several lines of evidence

* Corresponding authors.
E-mail addresses: hkj@nwu.edu.cn (K.-J. Huang), luochongguang@vip.gyig.ac.cn (C. Luo).

https://doi.org/10.1016/j.chemgeo.2021.120565
Received 15 March 2021; Received in revised form 22 September 2021; Accepted 7 October 2021
Available online 9 October 2021

support this hypothesis. First, ejecta weathering and/or more intense volcanic activity during the early Earth favor the accumulation of bicarbonate and the consumption of calcium, building a "soda ocean" based on thermodynamic, kinetic, and mass balance considerations (Kempe and Degens, 1985; Kadoya et al., 2020). Second, the extensive distribution of primary sedimentary minerals of dolomite, magnesite, and nahcolite in Precambrian and the lack of massive gypsum/anhydrite deposition before 1.8 Ga imply both the high alkalinity and low calcium concentration in the early oceans (Tucker, 1982; Grotzinger and Kasting, 1993; Lowe and Worrell, 1999; Frank and Fielding, 2003; Sugitani et al., 2003). Third, "soda oceans" with high alkalinity and low Ca concentration could chemically facilitate the biogenesis because low calcium prevents the binding of Ca^{2+} onto phosphate and high alkalinity promotes the synthesis of polypeptides (Kempe and Kazmierczak, 1994, 2011).

Some mineralogical and geochemical studies on the Precambrian sediments, however, largely disapprove of the SOH. The positive cerium anomalies and positive nitrogen isotope signatures in modern soda lakes are not observed in Archean marine sedimentary rocks, indicating the absence of high alkalinity in the Archean oceans (Bau and Dulski, 1996; Stüeken et al., 2015). Furthermore, the moderate Ca/ALK ratios inferred from the small calcium isotope variability in evaporitic sedimentary carbonates between 2.7 and 1.9 Ga also contradict the SOH (Blättler et al., 2016). Overall, discrepancies between current understandings on Precambrian seawater chemistry and SOH requires additional evidence to provide further insights.

The mineralogy and geochemistry of evaporites usually provide critical information for constraining the ancient seawater compositions. For example, the late-stage Mg-sulfates were used to distinguish the Phanerozoic "aragonite seas" and "calcite seas" (Hardie, 1996). Archean "soda oceans" is supposed to produce evaporites of nahcolite and trona (Warren, 2016), which is different from the common Phanerozoic marine evaporites, providing a clue to test the "soda ocean" using evaporites. Therefore, detailed investigations on the mineralogy and geochemistry signatures of "soda ocean" -derived evaporites can be applied to diagnosing the Precambrian "soda oceans". Here, Qinghai Lake (QHL), a modern soda lake with a composition of $Ca^{2+} << HCO_3^-$ (Sun et al., 1995, 2002; Jin et al., 2010), was used to conduct the evaporation experiment. Because of the high Mg content in Ca-depleted QHL (~760 ppm) and the significant Mg isotopic fractionation between brine and evaporites (Li et al., 2011; Feng et al., 2018; Shalev et al., 2021), the characterization of mineralogy and Mg isotope fractionation of evaporites are expected to provide useful hints on fingerprinting the "soda oceans" evaporitic deposits. Our results show that the residual brine is gradually enriched in ^{26}Mg during evaporation as the degree of evaporation (DE) increases due to the preferential incorporation of light Mg into evaporites (hydrous Mg-carbonates, halite, and bloedite in sequence). Particularly, massive precipitation of Mg-rich carbonates and significant Mg isotopic variation within those earliest evaporites may serve as an archive for diagnosing the high alkalinity and low calcium of the Precambrian "soda oceans".

2. Geological setting and sampling

QHL is located at the northeastern of the Tibet Plateau (36°32′–37°15′N, 99°36′–100°47′E) with an altitude of ~3190 m (Fig. 1A). As the largest brackish and inland lake in China, it has a surface area of 4400 km^2 and a water volume of 71.6 × 10^9 m^3 with an average depth of 21 m (e.g., Cui et al., 2016).

The mean annual temperature in the QHL drainage basin is ~ −0.1 °C, and the mean annual precipitation and evaporation are ~373 mm and 800 to 1100 mm respectively, with more than 80% precipitation and 60% evaporation occurring between July and September (An et al., 2012). Intense evaporation under the semi-arid environment and no surface outflows result in continual consumption of Ca and constant accumulation of Mg and HCO_3 in the QHL through the precipitation of aragonite (Li et al., 2007). The present-day QHL water has a pH of ~9.2, and relatively high [HCO_3] of 770 ppm, low [Ca] of 10 ppm, and high Mg/Ca of ~72 in the mass ratio (Sun et al., 1995, 2002; Cui et al., 2016) (Table A1). Several tributaries drain into the QHL, and the largest one, the Buha river (BHR), which makes up >50% of the total fluvial input, has a chemical composition of $Ca^{2+} << HCO_3^-$ (Fig. 1B). About 50 L of QHL water was pumped and passed through a 0.45 μm nylon filter at the South bank, Erlangjian hydrologic station of the QHL on January 26, 2015 (Fig. 1A). Besides, around 10 lL of BHR water was also collected and filtered at the same time to represent the fluvial inflow of QHL.

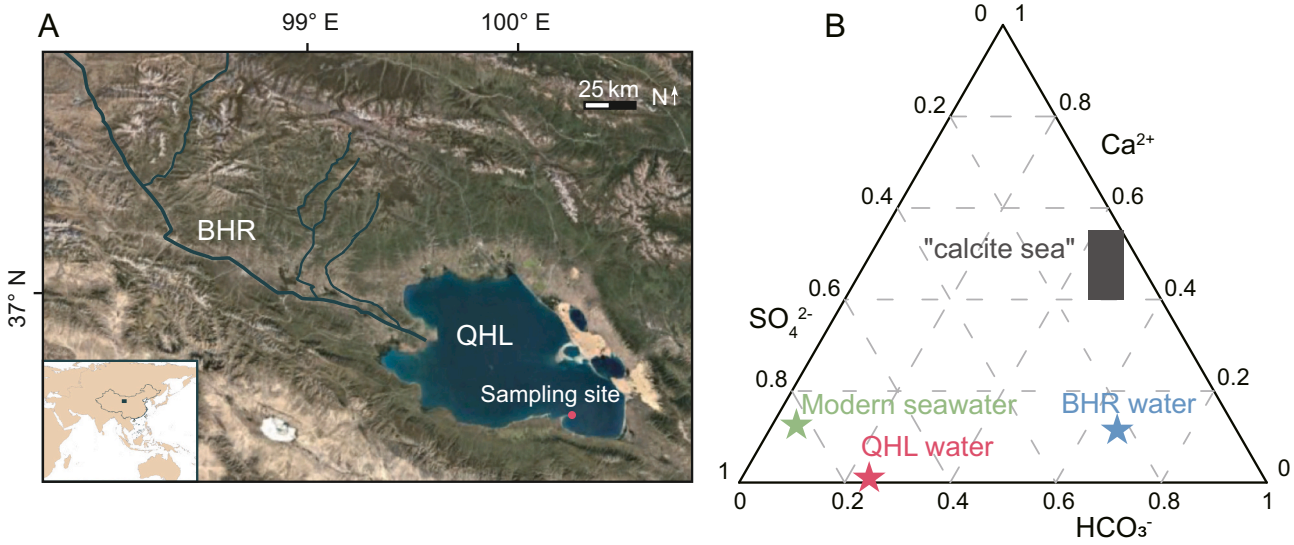

Fig. 1. (A) Geographic location of QHL and sampling site. (B) The ternary diagram shows the chemical composition of the QHL, BHR, modern aragonite sea and historical "calcite sea". "Calcite sea" is from the geological period that the marine abiotic limestones are dominated by low-Mg calcite instead of aragonites (Hardie, 1996), and the chemical composition is from Horita et al. (2002), details see in Table A1.

3. Methods

3.1. Evaporation experiment

A rough evaporation path of the QHL water was previously investigated by Sun et al. (1995, 2002), and the mineralogy of the evaporitic sequence was determined (Table A2). In this study, a similar but more detailed evaporation experiment of the QHL water was conducted at the laboratory of the State Key Laboratory of Ore Deposit Geochemistry (SKLODG), Guiyang, China.

Total 45 L QHL water, which was collected from the same location as in Sun et al. (1995, 2002), was firstly pre-concentrated to high salinity brine using a large plastic container under 25 °C in the lab, and about 1.3 L condensed brine (CB) was obtained after a two-week pre-concentration. A bulk precipitate sample (CBC) during this stage was collected for analysis. Later, two 2 L-graduated clean beakers, labeled as L and R groups, were filled with equal amounts of CB (about 640 mL) and placed on a hotplate under 28 ± 2 °C and normal pressure to simulate natural evaporation (see illustration in Fig. 2). A watch glass was placed in the beaker and removed from the beaker as soon as a sufficient amount of precipitate (~0.5 g) was formed on it (generally 1–2 days); simultaneously, ~1 mL liquid sample was collected. The watch glass was replaced once precipitate had been extracted, and the collected precipitate was rinsed with acetone at least three times to remove the absorbed brine and then air-dried. The pH of the brine was measured at the same time. Limited sample removal maintained the system stable. A total of eight solution and eight precipitate samples were collected from each group respectively, and the precipitates were allowed to accumulate on the bottom of the beakers as brine evaporating until the brine left in the beaker was insufficient to continue the evaporation experiment.

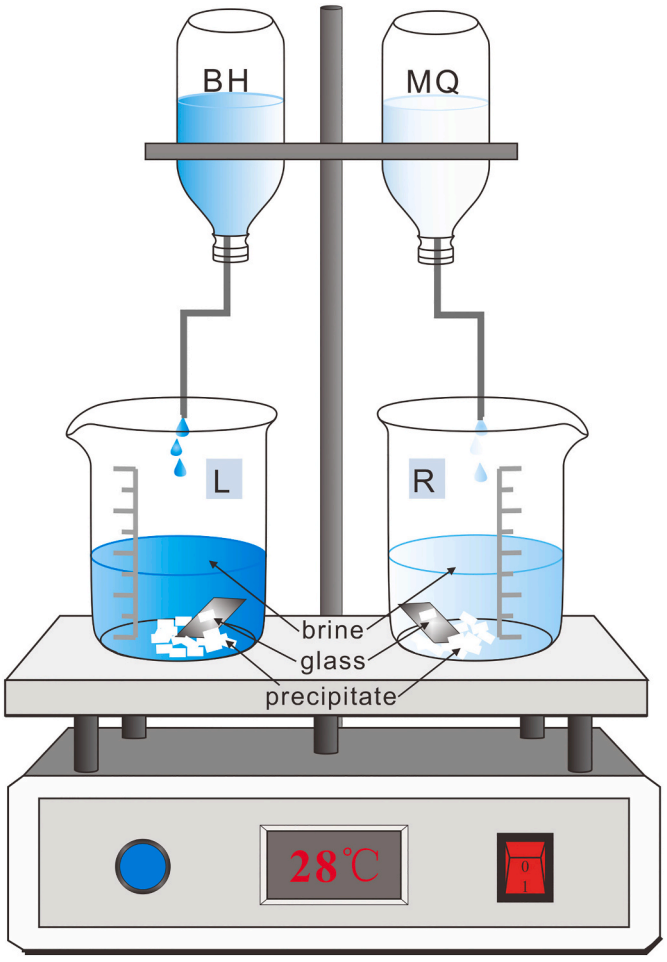

Fig. 2. Illustration of the evaporation experiment. L and R groups are heated on the hot plate at 28 °C after pre-concentration, the glass is placed for the collection of solid and the majority of solid is reserved at the bottom of the beakers. The fluvial discharge is added by two hanging droppers filled with BHR water (L group) and Milli-Q water (R group) respectively during dilution.

The following dilution operation was carried out by two hanging droppers filled with BHR water (L group) and Milli-Q water (R group) respectively, simulating the natural fluvial discharge (Fig. 2). BHR water represents the river runoff that flows into the QHL and Milli-Q water was used as a control group to study how the evaporation process is affected by the BHR. The droppers were controlled to ensure the recharge rate was constant and higher than the evaporation rate. The same sample collection protocol was applied during the dilution, and four solution and four precipitate samples were collected from each group for analyses. The total evaporation experiment lasted one and a half months.

3.2. Mineralogical and elemental analyses

Mineralogical and elemental analyses were conducted at the SKLODG. The mineralogy of precipitate samples was measured by X-ray Diffraction (XRD). About 0.2 g powdered sample was loaded into a glass sample holder with a flat surface that smoothed by a piece of glass. The working voltage and current were set at 40 kV and 40 mA. The diffraction spectral pattern was measured at a 2θ step of 0.02° between 4° and 60° with Ni-filtered Cu K_α radiation.

10.3 mg solid samples were weighted and dissolved in 1 mL 3% distilled nitric acid (HNO_3), and then diluted for chemical analysis. Aliquots of brine samples were pipetted and dried, and then dissolved in 3% HNO_3 for chemical analysis. Elemental compositions of cations were measured by an inductively coupled plasma atomic emission spectroscopy (ICP-AES, Varian VISTA) with analytical reproducibility (2σ) of ±5%. The contents of anions were determined by ion chromatography (IC, ICS900) with a 2σ of ±2%.

3.3. Mg isotope analyses

Magnesium isotopic analyses were performed at the State Key Laboratory of the Continental Dynamics (SKLCD), Northwest University, China. All chemical purifications were conducted in the ultra-clean lab. Detailed methods of sample digestion, column chemistry, and isotopic analyses have been reported in previous studies (Bao et al., 2019, 2020); as such, only a brief description is provided below.

Samples that contain 10–40 μg Mg were dried down and then dissolved by 12 N distilled HCl. Two columns filled with Bio-Rad AG50W-X12 resin (200–400 mesh) were used to separate Mg from matrix metals. Column #1 was filled with 2 mL resin was designed to separate Mg from Ca. Then column #2 was filled with 0.5 mL resin was used to separate Mg from other matrix metals. Each column was processed at least twice for all samples to make sure the complete removal of the matrix metals. At least two standard materials (Seawater, BCR-2, or BHVO-2) were processed along with samples for each batch of column procedure. All separated Mg solutions were collected in screw-top Savillex vails and then dried down on a 120 °C-hotplate before finally dissolved in 3% HNO_3 for isotopic measurement. It should be noted that some samples have high Na/Mg in the mass ratio (up to around 400), which requires effective elution of Na in column chemistry. We synthesized samples contain 10 μg Mg with Na/Mg mass ratio of 400 to pass column #2, and the recovery of Mg is 98% with < 0.1 Na/Mg after twice column. Such high recovery of Mg is sufficient to avoid measurable artificial Mg isotope fractionation during column chemistry.

Magnesium isotopic ratios were measured by a Nu Plasma II MC-ICPMS (Nu Instruments, Wrexham, UK) at the SKLCD. About 1 ppm purified Mg solution was introduced by a 'wet' plasma system to analyze the Mg isotopic ratios following the method reported by Bao et al. (2019). Three Mg isotopes (24, 25, 26) were determined simultaneously in separate Faraday cups (L5, Ax, and H5) under the low-resolution

mode and the blank for ^{24}Mg during the measurement was negligible (~2 mV) relative to the sample signal (~8 V). An in-house standard solution (GSB Mg, national standard solution materials of pure Mg) was used to calibrate the instrumental fractionation using the standard-sample-standard bracketing method (SSB). The measured Mg isotope ratios are reported in the delta notation (δ) as relative deviations to the DSM3 standard, and Mg isotope fractionation between phase A and B is expressed as their relative δ value:

$$\delta^{x}Mg\ (‰) = \left\{ \frac{\left({}^{x}Mg/{}^{24}Mg\right)_{sample}}{\left({}^{x}Mg/{}^{24}Mg\right)_{DSM3}} - 1 \right\} \times 1000 \quad (1)$$

$$\Delta^{x}Mg_{A-B} = \delta^{x}Mg_{A} - \delta^{x}Mg_{B} \quad (2)$$

where x means mass 25 or 26, $\Delta^{x}Mg_{A\text{-}B}$ means δ value difference of ^{x}Mg between A and B. Each sample was measured two to four times and the errors are reported as two times the standard deviations of the repeated measurements (2SD). The $\delta^{26}Mg$ and $\delta^{25}Mg$ values of GSB to DSM3 are −2.05‰ ± 0.05‰ and −1.06‰ ± 0.03‰ (Bao et al., 2020). The long-term internal precision based on replicate runs of DSM3 and GSB is 0.06‰ (Bao et al., 2019), and reference materials yield values identical to previous studies within 2SD (Table A3).

4. Results

4.1. Mineralogical composition of precipitates

Aragonite, hydrous Mg carbonates, halite, thenardite, bloedite, epsomite, and carnallite precipitate in sequence during QHL water evaporation (Sun et al., 1995, 2002; Table A2). Our experiments obtained similar results in the evaporite sequence. The precipitates during pre-concentration mainly consist of halite, thenardite and hydrous Mg carbonates. The hydrous Mg carbonates are mainly hydromagnesite, because hydromagnesite and nesquehonite are Mg-bearing minerals that precipitate prior to halite saturation (Table A2), and CBC has [Mg]/[CO_3] similar to that in hydromagnesite while has no HCO_3 (Table A4). L and R group precipitates display identical variations in their mineralogical composition during the subsequent evaporation and fluvial dilution (Table A4). During evaporation, the first four precipitates mainly consist of halite, while the following four samples contain mainly halite with a minor amount of bloedite (Fig. 3 & Table A4). During dilution, the first (L9/R9) sample contains halite and bloedite, and the last three precipitates are halite (Fig. 3 & Table A4).

4.2. Elemental compositions of precipitate and brine

The concentrations of Mg, Na and B in the initial QHL water were ~760 ppm ~3900 ppm, and ~12 ppm respectively (Fig. A1 & Table A5). The ternary diagrams show that QHL water has higher bicarbonate while lower calcium than that of modern "aragonite sea" and historical "calcite sea" (Fig. 1B). Compared to the initial QHL water, ion concentrations in CB have increased more than fifteen times during the pre-concentration (Fig. A1 & Table A5). The concentrations of Mg, K, and B in brine increased more than twice compared to that of CB during subsequent evaporation, while Na, S, and Ca fluctuated within relatively narrow ranges (Fig. A1 & Table A5). Most of the ion concentrations in brine gradually decreased to near the values of CB after dilution (Fig. A1 & Table A5). Precipitates have relatively high Na while low Mg and S concentrations, which all display similar trends as those in brines (Table A4).

To evaluate the relative enrichment and depletion of elements in brine during the evaporation, we use a reference element B (Boron) with the following equation since no B-bearing mineral precipitate during our experiment:

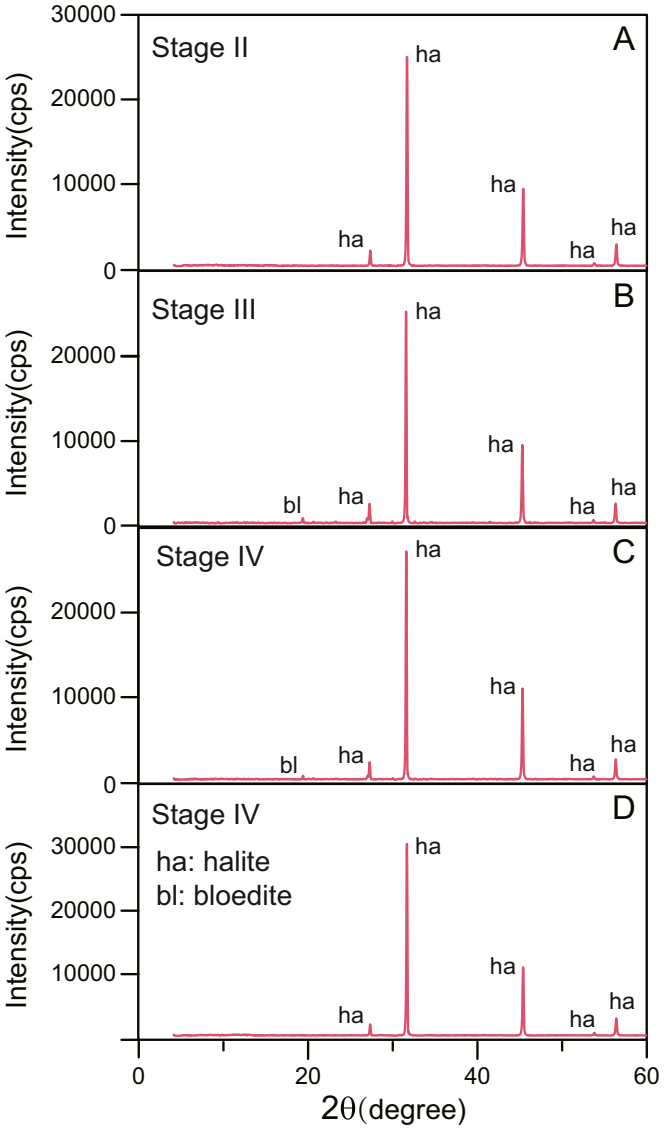

Fig. 3. X-ray diffraction pattern of the representative samples during each stage of the evaporation experiment. Note that the precipitate in Stage I was not measured for the mineralogy, and Stage IV has two types of precipitates, with or without bloedite.

$$X_n = (X/B)_{sample} \Big/ (X/B)_{QHL} \quad (3)$$

where $(X/B)_{sample}$ and $(X/B)_{QHL}$ refer to the concentration ratio of element X to B in the sample and QHL water respectively. $X_n < 1$ reflects the removal of elements from brine and $X_n > 1$ reflects the accumulation of elements in brine. Based on XRD and X_n results, the whole experiment can be divided into four stages (Figs. 3 & 4): hydrous Mg-carbonates precipitation (Stage I), halite precipitation (Stage II), bloedite precipitation (Stage III) and the dilution stage (Stage IV). The dramatic decrease of Mg_n and S_n indicates the precipitation of hydrous Mg-carbonates and thenardite within Stage I, and then Na_n decreased dramatically in Stage II. The slight enrichment of Na in Stage I is not surprising since B may be not conservative during this stage. The subsequent Stage III precipitates halite and bloedite with large depletion of all elements, which then all roughly recovered during Stage IV (Fig. 4).

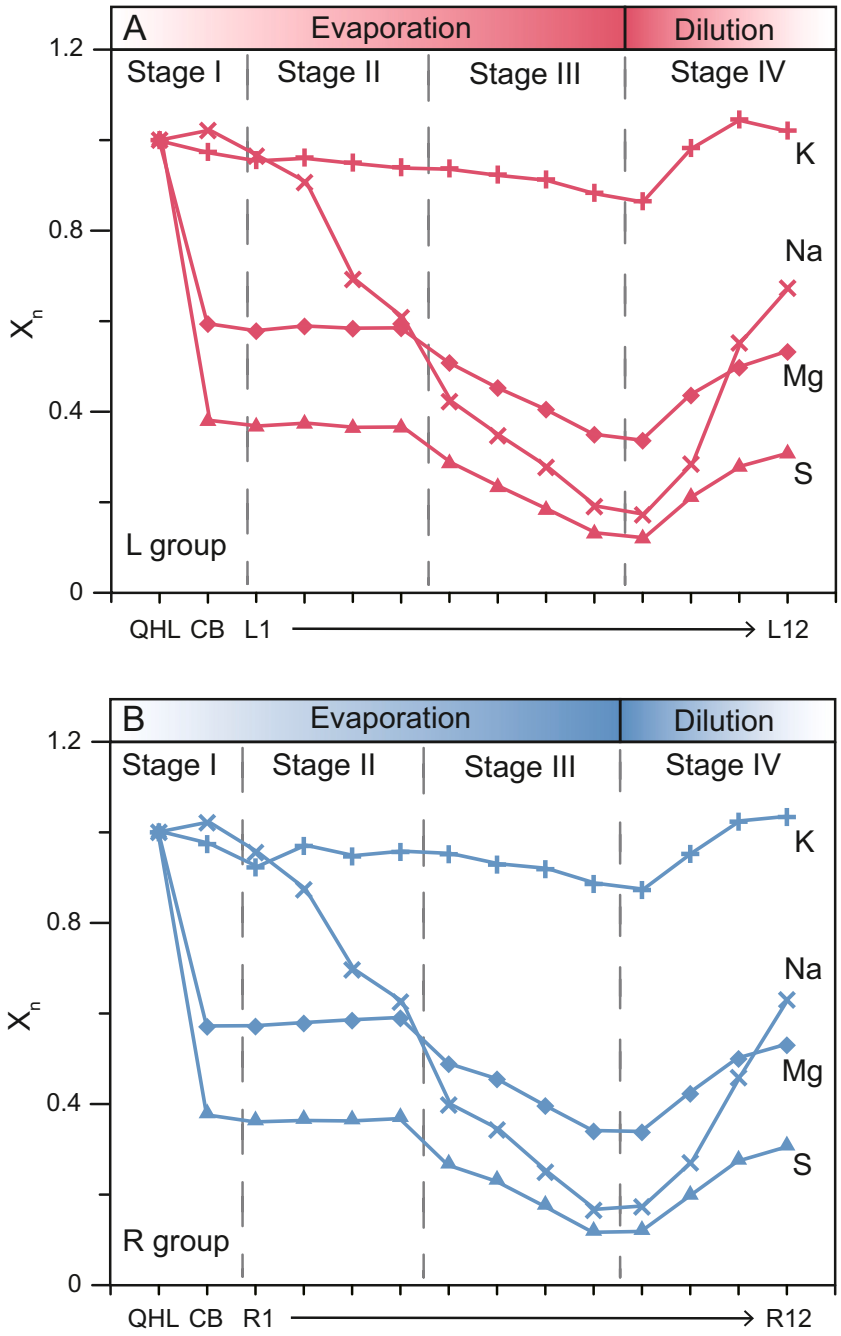

Fig. 4. The relative enrichment or depletion of elements in brine (X_n) during the brine evaporation experiments of (A) L group and (B) R group.

4.3. Degree of evaporation (DE)

DE is usually defined as the mass ratio of the original and remaining solution to describe the evolution of evaporation, and elemental concentration ratios are also proposed for additional constraints because the solution volume is not always accessible (Bąbel and Schreiber, 2014). The lack of reliable DE data owing to the retaining of the solid phase in evaporating brine leads us to use a modified DE' to evaluate the evaporation process:

$$DE' = 34.6 \times B_{sample}/B_{CB} \quad (4)$$

where B_{sample} and B_{CB} represent B concentration in sample and CB, respectively, and 34.6 is DE in the pre-concentration stage. The fraction of Mg remaining in brine (F_{Mg}) can be calculated through DE' and Mg concentration:

$$BV = 1/DE' \quad (5)$$

$$F_{Mg} = BV \times C_{Mg}/Mg_0 \quad (6)$$

where BV, C_{Mg}, and Mg_0 denote the residual brine volume, the concentration of Mg, and the starting mass of Mg respectively. Since B in brine was only concentrated by ~23 times when DE reached 34.6 (1.3 L CB from 45 L QHL water) during pre-concentration, and B can be incorporated into solid during brine evolution (Vengosh et al., 1992), this evaluation would underestimate DE and overestimate F_{Mg}. Therefore, the relationship between DE and DE_B in Vengosh et al. (1992) can be used to give an estimation of the actual DE and F_{Mg} (DE" and F_{Mg}", see in Table 1). Sixty percent Mg has been removed to precipitate during

Table 1
Chemical and Mg isotopic compositions of solution and precipitate.

Sample	DE"	F_{Mg}"	K_n	Mg_n	Na_n	S_n	pH	IS (M) [1]	Mg (molality)	δ^{25}Mg (‰)	2SD	δ^{26}Mg (‰)	2SD
Solution													
BHR								0.007	0.0004	−0.66	0.01	−1.28	0.02
QHL	1.00	1.000	1.000	1.000	1.000	1.000	9.20	0.25	0.03	−0.80	0.03	−1.51	0.03
CB	34.6	0.396	0.974	0.594	1.021	0.380		4.98	0.63	−0.24	0.04	−0.44	0.05
L1	51.4	0.346	0.956	0.578	0.965	0.367	7.66	6.05	0.90	−0.20	0.10	−0.35	0.08
L2	47.1	0.352	0.962	0.588	0.906	0.374	7.62	5.52	0.80	−0.20	0.05	−0.35	0.04
L3	60.4	0.347	0.950	0.583	0.692	0.364	7.54	5.59	0.84	−0.17	0.01	−0.35	0.01
L4	62.0	0.346	0.940	0.584	0.608	0.365	7.51	5.45	1.04	−0.16	0.00	−0.33	0.06
L5	105.7	0.279	0.938	0.508	0.422	0.286	7.43	5.86	1.48	−0.08	0.04	−0.15	0.07
L6	123.8	0.240	0.924	0.452	0.347	0.233	7.42	5.74	1.47	−0.04	0.06	−0.06	0.03
L7	166.0	0.200	0.913	0.404	0.277	0.183	7.37	5.84	1.64	0.05	0.01	0.11	0.01
L8	260.8	0.151	0.884	0.349	0.190	0.131	7.37	6.05	1.96	0.10	0.04	0.19	0.07
L9	266.7	0.144	0.865	0.336	0.172	0.120	7.35	5.88	1.90	0.03	0.04	0.10	0.03
L10	145.3	0.223	0.983	0.436	0.284	0.212	7.41	5.66	1.60	−0.03	0.02	−0.03	0.03
L11	78.3	0.287	1.046	0.497	0.552	0.278	7.62	5.80	1.12	−0.09	0.04	−0.22	0.03
L12	60.4	0.316	1.021	0.532	0.673	0.308	7.62	5.72	0.94	−0.15	0.04	−0.32	0.05
R1	48.5	0.342	0.923	0.571	0.955	0.364	7.64	5.87	0.83	−0.24	0.04	−0.42	0.03
R2	51.4	0.346	0.970	0.578	0.873	0.367	7.66	5.74	0.87	−0.21	0.04	−0.39	0.04
R3	62.0	0.346	0.947	0.584	0.696	0.366	7.55	5.89	1.08	−0.18	0.01	−0.34	0.03
R4	48.5	0.353	0.957	0.589	0.625	0.371	7.51	5.28	0.82	−0.19	0.03	−0.37	0.02
R5	101.9	0.270	0.952	0.488	0.398	0.269	7.45	5.81	1.38	−0.08	0.00	−0.12	0.03
R6	125.9	0.241	0.929	0.454	0.343	0.233	7.41	5.88	1.40	−0.04	0.02	−0.07	0.03
R7	168.3	0.195	0.919	0.396	0.249	0.178	7.32	6.00	1.67	0.01	0.04	0.00	0.04
R8	309.3	0.139	0.886	0.339	0.165	0.120	7.29	6.46	2.25	0.04	0.03	0.10	0.02
R9	260.8	0.146	0.873	0.337	0.173	0.122	7.29	6.11	1.94	0.04	0.02	0.07	0.02
R10	149.8	0.215	0.952	0.422	0.270	0.200	7.50	5.99	1.66	−0.01	0.02	−0.03	0.05
R11	94.4	0.281	1.024	0.500	0.458	0.277	7.58	5.60	1.29	−0.15	0.01	−0.26	0.08
R12	70.0	0.311	1.034	0.530	0.630	0.308	7.58	5.79	1.08	−0.15	0.02	−0.30	0.02
Precipitate													
CBC										−1.21	0.02	−2.30	0.01
L1C										−0.11	0.04	−0.02	0.09
L2C										−0.30	0.04	−0.57	0.07
L3C										−0.36	0.05	−0.60	0.04
L4C										−0.30	0.03	−0.55	0.05
L5C										−0.50	0.00	−0.97	0.07
L6C										−0.51	0.06	−1.01	0.12
L7C										−0.48	0.10	−0.90	0.23 [2]
L8C										−0.22	0.03	−0.46	0.11
L9C										−0.19	0.08	−0.35	0.17
L10C										−0.06	0.04	−0.04	0.06
L11C										0.02	0.06	0.03	0.07
L12C										−0.19	0.07	−0.40	0.08
R1C										−0.05	0.03	−0.08	0.10
R2C										−0.31	0.01	−0.56	0.04
R3C										−0.33	0.04	−0.59	0.09
R4C										−0.34	0.04	−0.64	0.06
R5C										−0.57	0.04	−1.08	0.11
R6C										−0.52	0.02	−0.98	0.04
R7C										−0.47	0.05	−0.91	0.07
R8C										−0.40	0.04	−0.77	0.08
R9C										−0.26	0.07	−0.51	0.07
R10C										−0.09	0.05	−0.10	0.10
R11C										0.07	0.09	0.00	0.10
R12C										−0.12	0.07	−0.24	0.05

[1] IS shorts for ionic strength, which is determined by the total dissolved constituents in the solution.
[2] Note that L7C has an unexpectedly high deviation, while which does not influence the major issues we discussed.

pre-concentration. Then F_{Mg} and F_{Mg}" remained consistent during halite precipitation and decreased to 22% and 14% respectively after bloedite precipitate (Tables 1 & A6). DE' reached around 180 at the most evaporated samples (R8 and L9) and finally decreased to ~60 as a result of dilution (Table A6), while DE" shows higher values up to 266 and 309 for L and R groups respectively (Table 1). Considering the incorporation of B into precipitate, DE" and F_{Mg}" are closer to the actual values.

4.4. Mg isotopic compositions of precipitate and brine

CB has a δ^{26}Mg value of −0.44‰, which is significantly higher than that of the initial QHL water of −1.51‰ (Fig. 5). Brines in both L and R groups display similar Mg isotopic variations during the subsequent evaporation and dilution (Fig. 5). The δ^{26}Mg values of the initial brine are identical (−0.35‰ for L group and −0.42‰ for R group) to that of CB within errors and maintain relatively invariant in Stage II (Fig. 5). Subsequently, brines become gradually enriched in heavy Mg isotopes in Stage III for both groups and their δ^{26}Mg values increase up to 0.19‰ for L group and 0.10‰ for R group, and then finally decrease to ~ −0.30‰ in Stage IV (Fig. 5).

Compared to the corresponding brine, most precipitates have relatively lower δ^{26}Mg values except for two samples in L group (L1, L11) and two samples in R group (R1, R11) (Fig. 5). The bulk precipitate sample in Stage I has a significantly low δ^{26}Mg value of −2.30‰. Precipitates in Stage II have constant δ^{26}Mg values, which are generally lower than that of contemporaneous brine by ~0.2‰ (Fig. 5). However, δ^{26}Mg values of precipitates gradually increase from ~ −1.05‰ (L5/R5) to 0.03‰ (L11) and 0.00‰ (R11) in Stage III, and finally decrease to

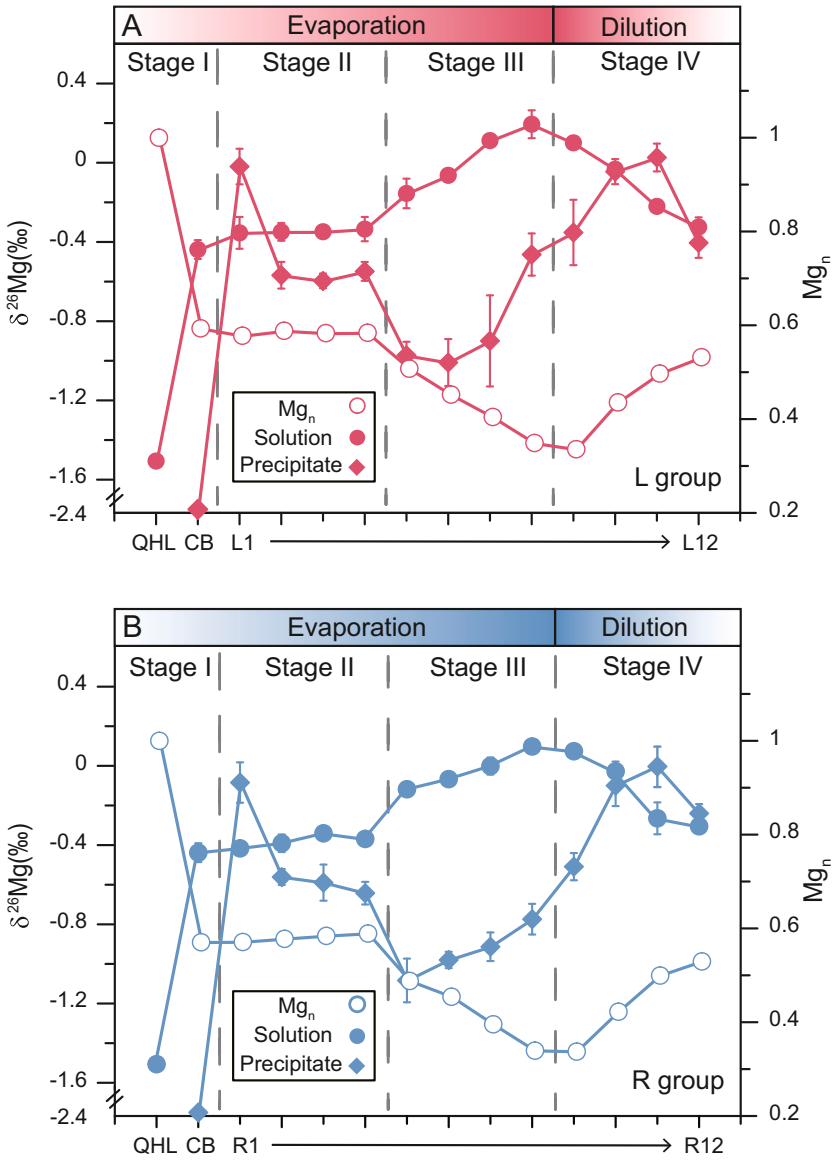

Fig. 5. The evolution of Mg_n in brine, as well as Mg isotopic compositions of brine and solid samples during the brine evaporation experiment for (A) L group and (B) R group. Error bars in this and subsequent plots represent two times the standard deviations (2SD).

−0.40‰ (L12) and −0.24‰ (R12) during the followingStage IV (Fig. 5).

5. Discussion

In this section, we first evaluate the evaporation path of QHL water, and then discuss the behavior of Mg isotopes during QHL water evaporation. Finally, we explore the potential implications of Mg isotopes on diagnosing the Precambrian "soda oceans".

5.1. Evaporation path of QHL water

There are mainly three types of evaporating brine according to the chemical divides and evaporation evolution path (Bąbel and Schreiber, 2014). Calcium and bicarbonate concentrations are firstly used to determine the brine toward alkaline or salt ($Ca^{2+} < HCO_3^-$ for alkaline and $Ca^{2+} > HCO_3^-$ for salt), and then calcium and sulfate concentrations further distinguish "calcite sea" ($Ca^{2+} > SO_4^{2-}$) from "aragonite sea" ($Ca^{2+} < SO_4^{2-}$). The evaporated products of waters are determined by the contemporaneous ion concentrations and the solubility of certain salt, and hence could largely reflect the initial chemical composition of water. The oscillation between "aragonite seas" and "calcite seas" of the Phanerozoic seawater is evidenced by the presence of Mg-sulfates in late-stage evaporites (Hardie, 1996), because the surplus SO_4^{2-} precipitate with Mg^{2+} to produce Mg-sulfates in $Ca^{2+} < SO_4^{2-}$ "aragonite seas". Modern "aragonite sea" is saturated with aragonite, and gypsum, halite, Mg-sulfate, sylvite, carnallite, as well as bischofite precipitate in sequence during evaporation. By comparison, evaporites formed in Phanerozoic "calcite seas" display similar evaporitic sequences but lack Mg-sulfates due to the low initial oceanic Mg/Ca ratio (Hardie, 1996). Theoretically, Precambrian "soda oceans" would precipitate nahcolite and trona along with halite but lack gypsum due to the high ALK and low Ca concentration (Lowe and Worrell, 1999; Sugitani et al., 2003; Warren, 2016).

As a soda lake, QHL has a chemical composition of $Ca^{2+} < HCO_3^-$, which is different from that of the Phanerozoic "aragonite seas" and "calcite seas", but possibly like the Precambrian "soda oceans" (Kempe and Degens, 1985; Warren, 2016). Calcium is rapidly consumed by bicarbonate through the precipitation of carbonates during the earliest QHL water evaporation. Subsequently, the redundant HCO_3^- co-precipitates with Mg^{2+} in the form of hydrous Mg-carbonates, such as

nesquehonite and hydromagnesite (Table A2), which are generally found in modern soda lakes (e.g., Power et al., 2019). Near unity (Ca + Mg)/HCO_3 ratio in QHL water facilitates the extensive and voluminous precipitation of hydrous Mg-carbonate minerals (Warren, 2010), which is different from the evaporation path of Phanerozoic seawater, in which gypsum would precipitate after the consumption of almost all bicarbonate through calcium carbonate precipitation (Bąbel and Schreiber, 2014). Consequently, a large amount of Mg is removed from QHL brine to carbonates before halite saturation, and then SO_4 accumulates in the brine and co-precipitates with Na, Mg, and K in the form of sulfate minerals during late-stage evaporation (Table A2).

Therefore, the evaporation path of QHL water overall covers the stages of carbonates, halite, Mg- and K-sulfates, as well as other chlorides precipitation (Table A2). Particularly, our experiments focus on the precipitation of hydrous Mg carbonates, halite, and bloedite stages which are accompanied by the considerable removal of Mg and hence could potentially fractionate Mg isotopes (Fig. 3 & Table A2). Below we discuss the behavior of Mg isotopes during QHL water evaporation in detail.

5.2. The behavior of Mg isotopes during QHL water evaporation

5.2.1. Hydrous Mg-carbonates precipitation (Stage I)

During the hydrous Mg-carbonate stage, the $\delta^{26}Mg$ value of brine becomes significantly higher than that of QHL water (Fig. 5). The enrichment of ^{26}Mg and decrease of Mg_n in brine suggest that light Mg isotopes prefer hydrous Mg carbonates (mainly hydromagnesite) to the brine (Fig. 5). This agrees with previous studies that the precipitation of nesquehonite and hydromagnesite preferentially incorporate the light Mg isotopes from the solution (Mavromatis et al., 2012; Shirokova et al., 2013; Oelkers et al., 2018; Harrison et al., 2021). A first-order mass balance calculation suggests that ~60% Mg in brine has been removed through carbonates precipitation, resulting in the remaining brine (CB) being 1.07‰ heavier than the QHL in $\delta^{26}Mg$ values (Fig. 5). To further understand the Mg isotope behavior during this stage, equilibrium fractionation and Rayleigh fractionation models are applied:

$$\delta^{26}Mg_b = \delta^{26}Mg_0 - \left(1 - F_{Mg}\right) \times \Delta^{26}Mg_{solid-solution} \quad (7)$$

$$\delta^{26}Mg_b = \left(\delta^{26}Mg_0 + 1000\right) \times {F_{Mg}}^{\alpha-1} - 1000 \quad (8)$$

where $\delta^{26}Mg_b$ and $\delta^{26}Mg_0$ refer to the $\delta^{26}Mg$ values of evaporating brine and QHL water, F_{Mg} represents the fraction of Mg in solution, and α is the Mg isotope fractionation factor between solid and solution. Eqs. (7) and (8) correspond to equilibrium fractionation and Rayleigh fractionation models respectively.

$\delta^{26}Mg$ value of the bulk precipitate sample during this stage is −2.3‰ (Table 1), which can be generated from the brine through both the Rayleigh and batch models (Fig. 6A). According to Eqs. (7) and (8), the average apparent $\Delta^{26}Mg_{solid\text{-}solution}$ of equilibrium fractionation and Rayleigh fractionation are −1.76‰ and −1.15‰ respectively (Fig. 6A). The latter value agrees with the reported $\Delta^{26}Mg_{solid\text{-}solution}$ of hydromagnesite (−0.9‰ to −1.1‰, Shirokova et al., 2013), indicating the removal of Mg from solution by Rayleigh distillation. Thus, the equilibrium fractionation between brine and precipitate would be obtained immediately after the hydromagnesite precipitation and no substantial reset of Mg isotopes during subsequent evaporation. This is consistent with the rapid equilibrium of Mg isotopes between hydrous Mg carbonates and solution in previous experimental studies (Oelkers et al., 2018; Harrison et al., 2021).

Such large Mg isotope fractionation in carbonates is not unusual, while evaporation can significantly remove brine Mg and thus make large $\delta^{26}Mg$ variation preserved in evaporites. However, brine $\delta^{26}Mg$ remains relatively consistent during modern seawater evaporation, especially in the earliest stages. This mainly attributes to the conservative behavior of Mg during evaporation when DE is below 100 (Xia et al., 2020; Shalev et al., 2021). The earliest evaporation yields constant $\delta^{26}Mg$ values in residual brine since there is no sizable Mg-bearing precipitate before DE approaches 60 (Shalev et al., 2021). Then the precipitation of epsomite and the subsequent kainite as evaporation have relatively small and opposite Mg isotope fractionation factors, so the brine $\delta^{26}Mg$ values remain within a narrow range around −0.8 ± 0.1‰ (Xia et al., 2020; Shalev et al., 2021). By contrast, the experimental evaporation of QHL water suggests that Mg isotope is projected to fractionate significantly during the earliest "soda ocean" evaporation, displaying > 1‰ $\delta^{26}Mg$ variation when DE is below 40 (Fig. 6B). The $\delta^{26}Mg$ variations of both the brine and precipitate are expected to be much larger during the potential "soda ocean" evaporation with lower Mg/CO_3, according to the similar distillation of calcium isotopes by bicarbonate in a modern alkaline lake (Nielsen and DePaolo, 2013) and calcium isotopes by sulfate in marine evaporitic gypsum (Blättler and

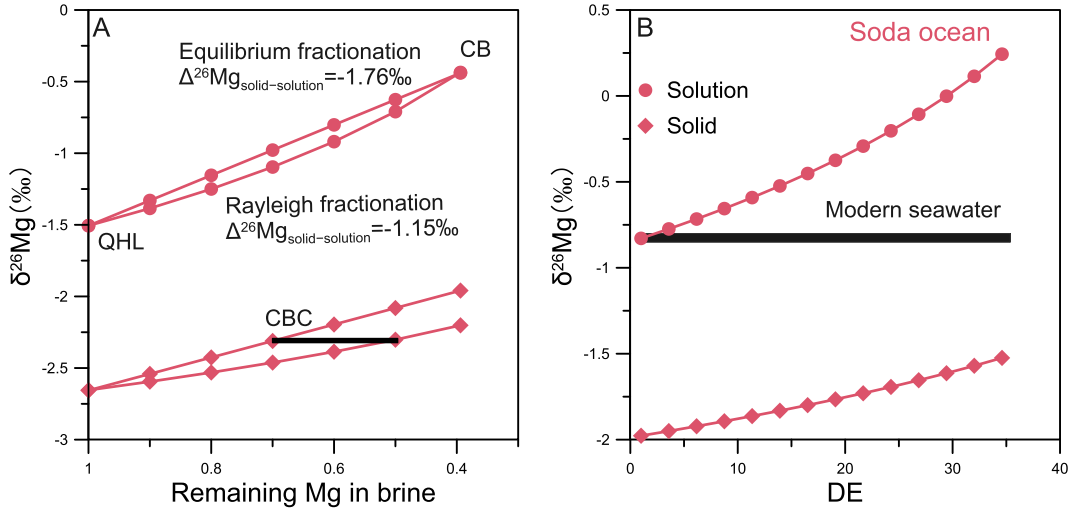

Fig. 6. (A) The evolution of brine and solid during Stage I, note that the brine can be modeled by both equilibrium fractionation (upper line) and Rayleigh fractionation (lower line) with different fractionation factors, and the representative precipitate sample can fit both models. (B) The $\delta^{26}Mg$ evolution during the earliest evaporation of modern seawater and "soda oceans". The modern seawater evolution curve is from Shalev et al. (2018, 2021) and Xia et al. (2020), where brine and evaporite have identical and consistent $\delta^{26}Mg$ values when DE is below 50. The pre-concentration stage of QHL water is supposed to represent the situation of the "soda ocean".

Higgins, 2014).

5.2.2. Halite precipitation (Stage II)

During Stage II, both the precipitates and brines have relatively constant $\delta^{26}Mg$ values, and the precipitates are slightly lighter or heavier than corresponding brines by ~0.2‰ (Fig. 5). Both precipitates and brines have narrow $\delta^{26}Mg$ value ranges, indicating Mg isotopes are not significantly fractionated. Such limited fractionation may be due to no substantial Mg-bearing mineral formation and/or near quantitative entrapment of brine Mg. Firstly, XRD screening indicates halite is the only detectable mineral during Stage II (Fig. 3). Further, Mg^{2+} in halite is commonly considered as a solute with other ions in fluid inclusions (McCaffrey et al., 1987), which is consistent with the low concentrations of Mg, Ca and SO_4 in precipitates (Table A4). Therefore, quantitative trapping of brine Mg into halite accounts for the limited isotopic fractionation. This is in agreement with the identical $\delta^{26}Mg$ value between Holocene halite and dead sea brine (Xia et al., 2020), further demonstrating the record of non-alkaline seawater Mg isotopic composition in halite. Besides, the fluctuation of halite $\delta^{26}Mg$ values may be owing to the entrapment of Mg-sulfates or carbonates. The co-precipitation of minerals with halite is common, considering the trace amount of Mg in halite, any trace amount co-precipitation of epsomite or carbonate, which has $\delta^{26}Mg$ values positive and negative than halite respectively (Li et al., 2011, 2012), would slightly alter the halite $\delta^{26}Mg$ values. This speculation is further supported by the presence of SO_4^{2-} and HCO_3^- in halite samples (Table A4).

5.2.3. Bloedite precipitation (Stage III)

The brines are gradually enriched in ^{26}Mg, indicating that light Mg isotopes are preferentially incorporated into the solid phase during Stage III (Fig. 5). Since bloedite is the exclusive Mg-bearing mineral in this stage, the Mg isotope fractionation between bloedite and brine ($\Delta^{26}Mg_{bloedite\text{-}brine}$) can be obtained as -0.86 ± 0.31‰ for the L group and -0.92 ± 0.08‰ for the R group. This fractionation fits better with the batch fractionation model (Fig. 7), indicating that Mg isotope fractionation of bloedite during evaporation is dominated by batch removal with an average $\Delta^{26}Mg_{bloedite\text{-}brine}$ of -0.89 ± 0.22‰.

The bonding environment of minerals, including the dehydration and Mg–O bond length, are previously suggested to have significant effects on Mg isotope fractionation between evaporitic minerals and solution (Li et al., 2011; Feng et al., 2018; Shalev et al., 2021). On one hand, Mg^{2+} in aqueous solutions is hydrated with each Mg^{2+} bonded to six H_2O molecules to form an octahedron of $[Mg(OH_2)_6]^{2+}$ (Schauble, 2011). The precipitation of minerals from the solution usually involves the dehydration of $[Mg(OH_2)_6]^{2+}$, for which prefer light Mg isotopes (Schauble, 2011; Mavromatis et al., 2012; Shalev et al., 2021). Because Mg in bloedite is octahedrally coordinated with four H_2O molecules and two oxygen atoms (Hawthorne, 1985), the dehydration of two H_2O molecules is required during the precipitation of bloedite from the evaporating brine. This process would account for the preferential incorporation of light Mg isotopes into bloedite, and roughly agrees with the previous studies (Fig. 8A). On the other hand, Mg isotope fractionation is also determined by the difference of Mg–O bond length between the mineral and solution. The shorter bond prefers heavy Mg isotopes to form stiffer bonds (e.g., Schauble, 2011; Shalev et al., 2021), hence longer Mg–O bond length resulting in more negative $\Delta^{26}Mg_{mineral\text{-}solution}$ values (Fig. 8B). Bloedite has an average Mg–O distance of 2.076 Å and a negative $\Delta^{26}Mg_{bloedite\text{-}brine}$ of -0.89 ± 0.22‰ (Hawthorne, 1985), which is in accordance with previous experimental data (Fig. 8B). The precipitation of hydromagnesite in Stage I follows a similar mechanism. The average Mg–O bond length in hydromagnesite is 2.08 Å and Mg in hydromagnesite is only bonded to one molecule H_2O (Akao et al., 1974), it has to dehydrate 5 molecules of H_2O to form hydromagnesite from the solution. The more H_2O molecules that are required to dehydrate and longer Mg–O bond length in hydromagnesite compared to bloedite likely account for the more enrichment of ^{24}Mg in hydromagnesite

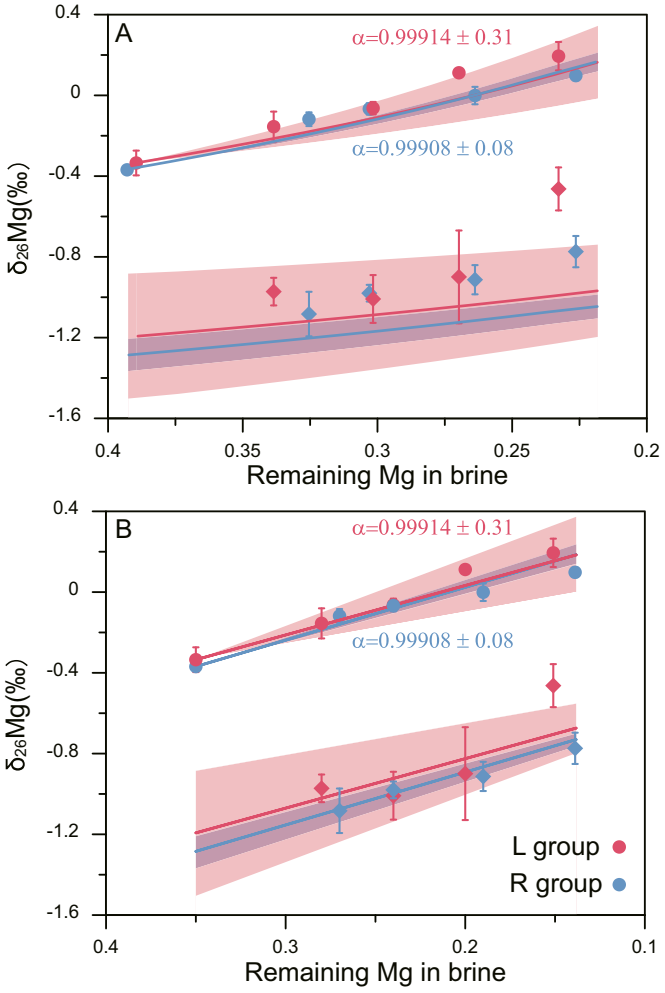

Fig. 7. $\delta^{26}Mg$ of brine and solid evolution during bloedite precipitation fitted by (A) Rayleigh fractionation model using F_{Mg} and (B) batch removal model using F_{Mg}". Red and blue color for L and R group respectively, and solid circles and diamonds represent brine and solid respectively. Red and blues lines represent the best fit, and the shadow covers the uncertainties of 2SD. Details of F_{Mg} and F_{Mg}" see in Table A6. (For interpretation of the references to color in this figure legend, the reader is referred to the web version of this article.)

(Shirokova et al., 2013) (Fig. 8A–B). Overall, Mg isotope fractionation between bloedite and brine during evaporation is mainly controlled by the bonding structure.

In addition to the bonding environment, ionic strength (IS) may also account for the $\Delta^{26}Mg_{bloedite\text{-}brine}$ variations in both L and R groups (Fig. 5). The increase of $\Delta^{26}Mg_{bloedite\text{-}brine}$ is accompanied by the enhanced molality of Mg and IS in solution, reflecting the potential influence of kinetic factors (Fig. 8C–D). The IS and ion concentrations increase as brine evaporation, likely resulting in the higher precipitate rate and smaller $\Delta^{26}Mg_{bloedite\text{-}brine}$. A similar effect of IS on Mg isotope fractionation has been observed during calcite precipitation, where $\Delta^{26}Mg_{mineral\text{-}solution}$ changed by ~1.3‰ when IS increases from 100 mM to 600 mM (Mavromatis et al., 2013). Therefore, the bonding structure determines the direction and scale of the $\Delta^{26}Mg_{bloedite\text{-}brine}$, while the kinetic effect in evaporated brine contributes to the variation of $\Delta^{26}Mg_{bloedite\text{-}brine}$.

5.2.4. Bloedite dissolution (Stage IV)

Ancient evaporites usually have undergone complex geological processes, which may introduce discrepancy and complexity when explaining the isotope data of evaporitic samples (e.g., Xia et al., 2020;

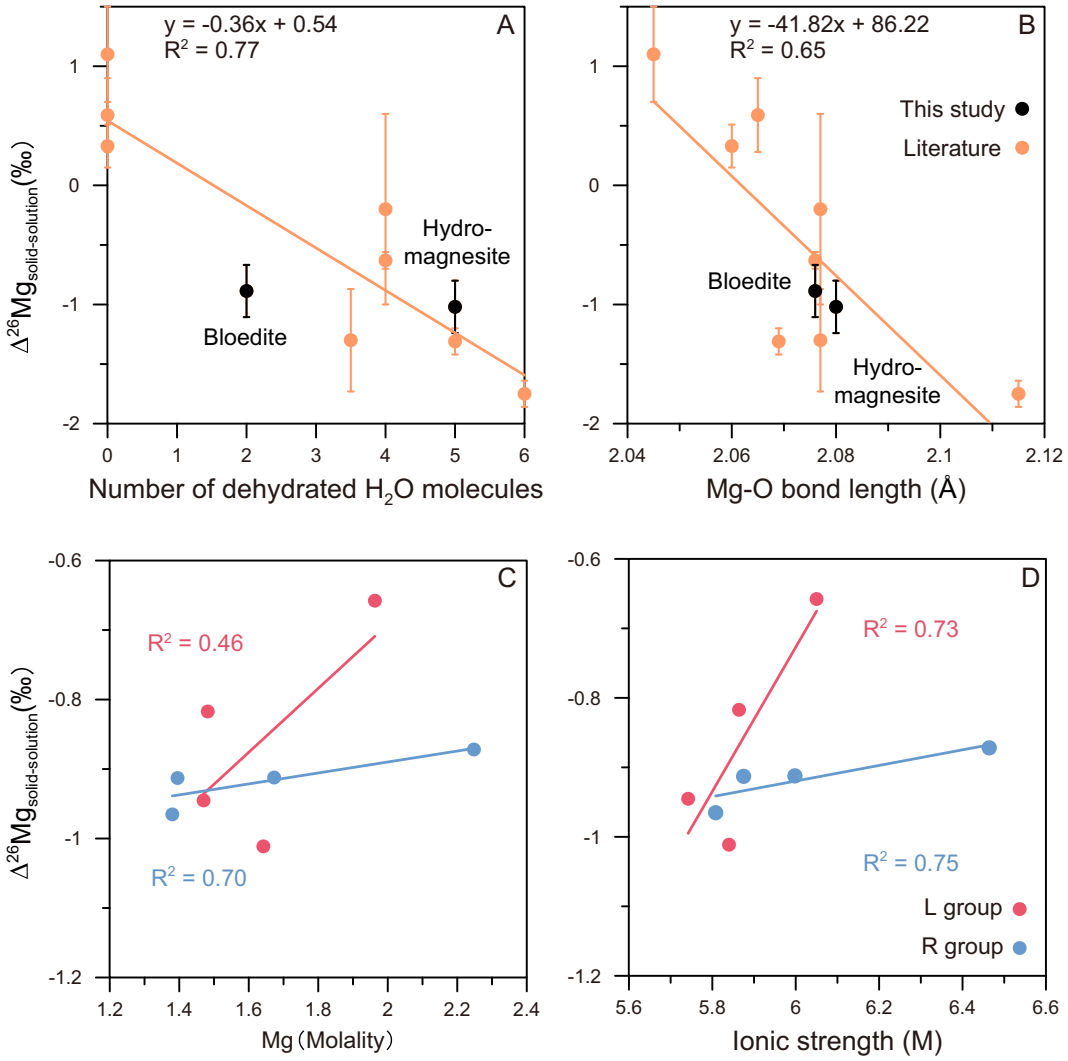

Fig. 8. $\Delta^{26}Mg_{solid\text{-}solution}$ versus (A) the number of dehydrated H_2O molecules to form a certain mineral, and (B) the Mg–O bond length. Crossplots between $\Delta^{26}Mg_{bloedite\text{-}brine}$ and (C) molality of Mg and (D) ionic strength in solution respectively. Detailed bond structure information sees in Table A7. The Molality of Mg and ionic strength in solution were calculated using PHREEQC V3 (Parkhurst and Appelo, 2013) and the LLNL database.

Shalev et al., 2021). One of the problems is the influx of meteoric water, which can potentially alter the composition of evaporating brine and therefore complicate the interpretation of ancient evaporitic sequences (Bąbel and Schreiber, 2014). In this study, fluvial recharge during Stage IV has limited influence on the mineralogy of precipitates but leads to an increase in Mg_n, Na_n, and S_n of brines (Fig. 4). Such an increase in brine major ions cannot be attributed to an additional input of ions during fluvial recharge, because Milli-Q water is substantially ion-free and ions in BHR are at least one magnitude lower than in QHL water (Table A1). More likely, the dissolution of pre-existing precipitates (mainly bloedite) accounts for the change of brine chemistry. Therefore, the evaporating brine is the binary mixture of the brine before this stage (L8/R8) and the dissolved solids. The behavior of Mg isotopes during the bloedite dissolution can be modeled by the Rayleigh distillation with various apparent fractionation factors (Fig. 9). Our modeling results show that the mixing line between brine and dissolved precipitates roughly encompasses the brine $\delta^{26}Mg$ value, indicating a relatively conservative behavior of Mg isotopes during the dissolution of precipitates (Fig. 9).

Such conservative behavior of Mg isotopes indicates the congruent dissolution of bloedite. This speculation is supported by the coordinating increase of Mg_n, Na_n and S_n (Fig. 4), as well as no change in mineralogical compositions of the precipitate. The congruent dissolution of carbonates is dynamic with reactions of both dissolution and re-precipitation; hence Mg isotope fractionation could arise from releasing, re-incorporation, and imbalance between these two processes (Pearce et al., 2012; Oelkers et al., 2018). Compared to the carbonate-solution systems, the recharging system in our experiment promotes a much more rapid dissolution of bloedite. Rapid dissolution minimizes the kinetic effects during both releasing and the reverse reactions and thus accounts for the conservative behavior of Mg isotopes. Besides, there are outliers off-track the model line in both groups (Fig. 9), which may be attributed to the heterogeneous Mg isotopic compositions of the solid phase. The binary mixing model assumed the precipitate as a homogeneous bulk solid phase, hence the dissolution of the pre-existing precipitates with different $\delta^{26}Mg$ values likely results in the deviation of brine $\delta^{26}Mg$ values from the model line.

The precipitate samples that mainly contain halite in Stage IV have $\delta^{26}Mg$ values close to the brine (Fig. 5), which is similar to Stage II. The first precipitate sample which contains bloedite has a smaller $\Delta^{26}Mg_{solid\text{-}solution}$ compared to that in the bloedite stage. This can be attributed to the unstable state of bloedite precipitation during dilution, which may alter the $\Delta^{26}Mg_{solid\text{-}solution}$.

5.3. *Implications for tracing ancient seawater chemistry*

Geochemical measurements and mineralogical observations of

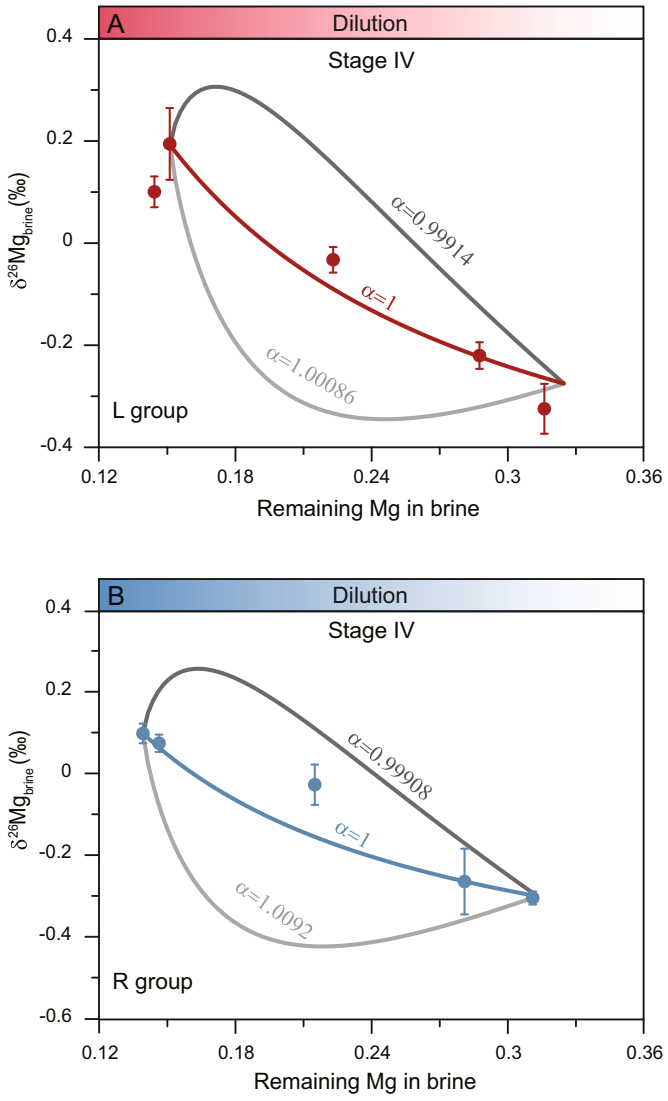

Fig. 9. Plotted and modeled brine $\delta^{26}Mg$ evolution during the dilution. A binary mixing model is used to match the brine $\delta^{26}Mg$ evolution: $\delta^{26}Mg_b = \delta^{26}Mg_0 \times (1-f) + \delta^{26}Mg_d \times f$; Rayleigh fractionation model is used to obtain the dissolved solid $\delta^{26}Mg$ value: $\delta^{26}Mg_d = (\delta^{26}Mg_s + 1000) \times f^{\alpha-1} - 1000$, where $\delta^{26}Mg_d$ and $\delta^{26}Mg_s$ here refer to the $\delta^{26}Mg$ values of dissolved solid and the bulk solid precipitated during Stages II and III. $\delta^{26}Mg_s$ is calculated by the total loss of Mg from brine and its $\delta^{26}Mg$. $\delta^{26}Mg_b$ and $\delta^{26}Mg_0$ refer to the evolving brine and the starting brine during this stage (L8/R8). f means the fraction of Mg dissolved from the solid accounts for the total Mg in evaporating brine.

sedimentary rocks indicate that seawater chemistry has significantly changed through Earth's history (Hardie, 1996; Lyons et al., 2014). It has been proposed that the alkalinity of Precambrian oceans was higher than that of modern seawater, which promotes biogenesis (Kempe and Degens, 1985; Grotzinger and Kasting, 1993). However, the appraisal of the seawater alkalinity of the early Earth has received limited attention so far due to the lack of reliable approaches.

Our study revealed that extensive hydrous Mg-carbonates precipitate during the earliest stages of alkaline brine evaporation, leading to significant Mg isotopic variation in evaporites. These observations provide important clues for discriminating the Precambrian "soda oceans" from the Phanerozoic "aragonite seas" and "calcite seas". Firstly, (hydrous) Mg-carbonate minerals including hydromagnesite, nesquehonite, dypingite, and magnesite, are very common in alkaline environments (Thompson and Ferris, 1990; Shirokova et al., 2013; Cangemi et al., 2016; Power et al., 2019). These Mg-carbonate minerals are also pervasively associated with microbial mats or cyanobacterials (Thompson and Ferris, 1990; Power et al., 2007; Shirokova et al., 2013; Sanz-Montero et al., 2019). Therefore, the existence of these minerals can be used as an indicator of both the high ALK and microorganism activities in the ancient ocean. Moreover, modeled brine $\delta^{26}Mg$ evolution during evaporation shows that "soda ocean" -derived brine (QHL water) displays a much larger $\delta^{26}Mg$ variation (> 1‰) than others in the earliest evaporitic deposits (Fig. 6B), this trend is also observed in the whole stage of simply modeled seawater $\delta^{26}Mg$ evolution during evaporation (Fig. 10). This large $\delta^{26}Mg$ variation can be available in the hypothetical Precambrian "soda oceans" with a lower Mg/HCO_3 ratio, according to the similar distillation of Ca isotopes by anions observed in both experiments and geological records (Nielsen and DePaolo, 2013; Blättler and Higgins, 2014). More importantly, the high $\delta^{26}Mg$ values accompanied by (hydrous) Mg-carbonates precipitation have been observed in modern alkaline lakes and playas (Shirokova et al., 2013; Mavromatis et al., 2021), demonstrating the distillation of Mg by alkalinity and the enrichment of heavy Mg isotopes through the precipitation of Mg-bearing carbonates. The playa that developed abundant hydromagnesite even documented the highest $\delta^{26}Mg$ value of carbonate so far (+ 2.2‰), which can only be resulted from the precipitation of hydromagnesite via Rayleigh distillation (Mavromatis et al., 2021). Similar conditions may also occur in the Proterozoic oceans where strata-bound magnesite deposits were developed, according to the abundance of magnesite, the large variation of $\delta^{26}Mg$ in magnesite (> 1‰) and the relatively high $\delta^{26}Mg$ value (mostly around −0.75‰, Dong et al., 2016). Although whether the magnesite precipitated from evaporating seawater or formed through the magnesitization of Mg-rich precursor remains controversial, either the scenario requires a high Mg and high alkalinity fluid chemistry to precipitate Mg-carbonates, which is favored in the Precambrian "soda oceans" instead of Phanerozoic-like seawater. Therefore, the high value and large variability of magnesite $\delta^{26}Mg$ potentially demonstrate the distillation of alkalinity to Mg in the hypothetical Precambrian "soda oceans".

The mineralogy and isotope signatures of hydrous Mg-carbonates as indicators of "soda oceans" may not be direct as calcium isotopic variation in evaporitic carbonates (Blättler et al., 2016). However, in contrast to the extremely low Ca concentration, Mg is likely more abundant in the "soda oceans" since the early crust is likely mafic and thus abundant Mg can be dissolved and transported into the ocean. Therefore, evaporitic hydrous Mg-carbonates may be much more common than evaporitic calcium carbonates in "soda ocean" deposits. Moreover, these minerals are enriched in Mg, suggesting the resistance to the alternations of the initial Mg isotopic signatures. The Mg isotope compositions of hydromagnesite from Atlin playas are well-preserved due to the large pool of Mg in hydromagnesite (Mavromatis et al., 2021), and $\delta^{26}Mg$ only changed by less than 0.2‰ during the experimental transformation of nesquehonite to dypingite from 5 to 35 °C (Harrison et al., 2021). These findings demonstrate that the initial Mg isotopic signatures of "soda oceans" stand a chance to be preserved. Furthermore, though the enrichment of ^{26}Mg in evaporites may also be derived from the change of seawater $\delta^{26}Mg$, the large $\delta^{26}Mg$ variation (~1‰) in brine and evaporites can still indicate the high alkalinity in Precambrian "soda oceans", comparing to the invariant $\delta^{26}Mg$ value in the earliest Phanerozoic "aragonite sea" and "calcite sea" evaporites (Figs. 6B & 10).

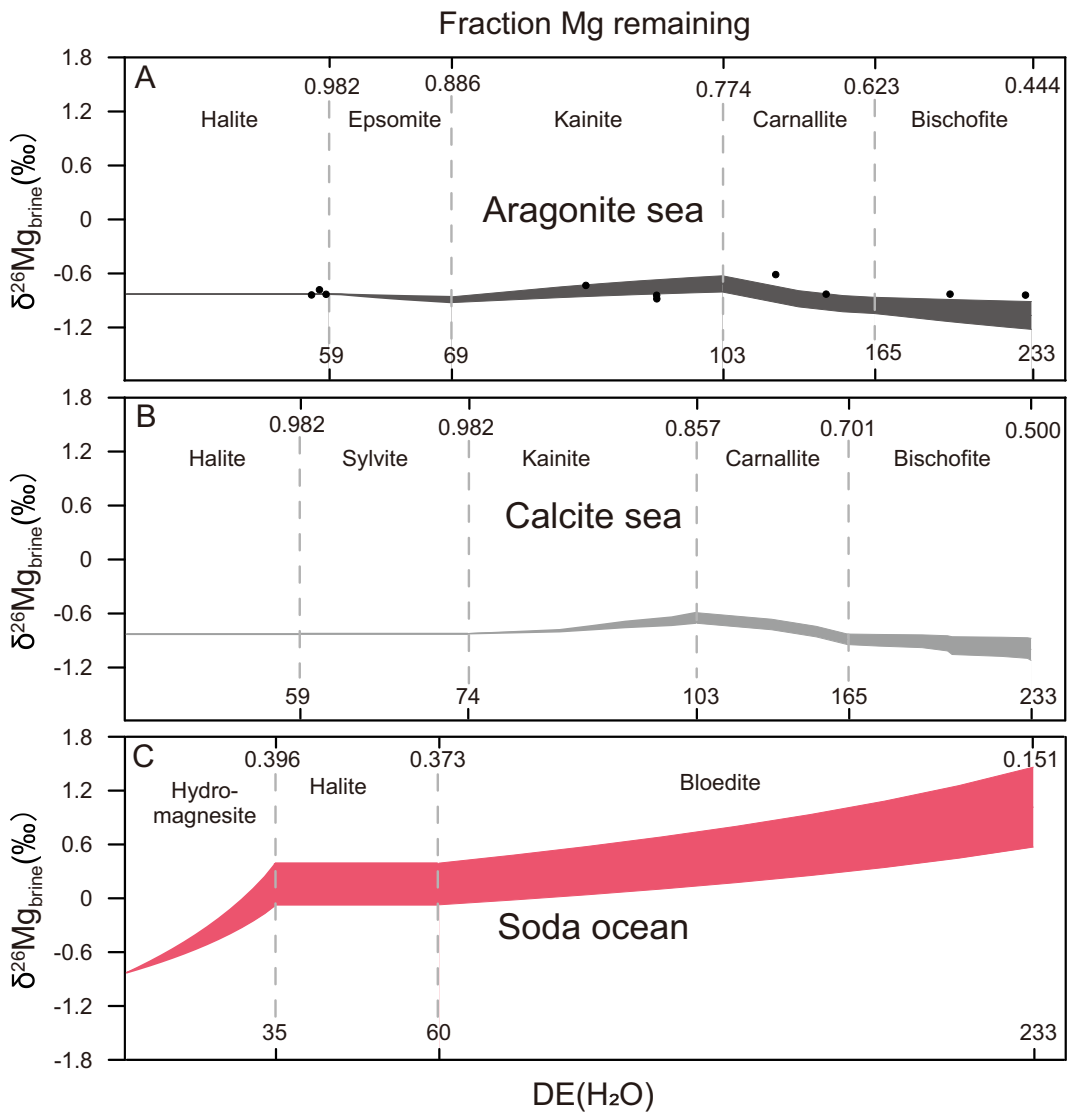

Fig. 10. Evolution of $\delta^{26}Mg_{brine}$ during evaporation with different initial seawater chemistry. The $\delta^{26}Mg$ value of primary seawater is assumed as the same as modern seawater from Ling et al. (2011). (A) F_{Mg} and DE of "aragonite sea" are from Shalev et al. (2018); (B) F_{Mg}, and DE of "calcite sea" are modified from Shalev et al. (2018); (C) F_{Mg} and DE of the "soda ocean" are from this study and Shalev et al. (2018). Only one dominated Mg-bearing mineral was assumed during a certain evaporation stage to simplify the calculation, and the evolving brine $\delta^{26}Mg$ value was calculated using the Rayleigh distillation model through Eq. (7). Hydrous Mg carbonate here is assumed as hydromagnesite, and the precipitation of halite and sylvite involve no Mg isotopes fractionation. Mg isotopes fractionation factors of other minerals can be seen in Table A7. Black dots in A are from Shalev et al. (2021), which roughly fit our simulation line.

6. Conclusions

To understand the behavior of Mg isotopes during alkaline brine evaporation and explore the utility of Mg isotopic composition of evaporites in testing the Precambrian "soda oceans", two sets of evaporation experiments using QHL water were conducted under 28 °C. Based on the mineralogical, chemical and Mg isotopic composition of brine and precipitate, our evaporation experiment involves the precipitation of hydrous Mg carbonates, halite, bloedite and the dissolution of bloedite. The precipitation of these evaporites removes up to 85% Mg from brine and leads to the successive enrichment of heavy Mg isotopes in brine. Voluminous precipitation of hydrous Mg-carbonates during the earliest QHL water evaporation in Stage I results in significant $\delta^{26}Mg$ variation (>1‰), which could potentially distinguish the Precambrian "soda oceans" from Phanerozoic seawater. Limited fractionation between brine and halite in Stage II indicates the archive of brine $\delta^{26}Mg$ in halite. The Mg isotopic composition of bloedite during evaporation in Stage III is mainly controlled by the bonding environment, including the dehydration and Mg–O bond length in bloedite, and less influenced by kinetics. Moreover, although the dissolution of bloedite in Stage IV is complicated with dynamic reactions and heterogeneous pre-precipitated components, Mg isotopes behaved conservatively due to the rapid dissolution. These findings not only elucidate the behavior of Mg isotopes during alkaline brine evaporation, but also provide novel insights into diagnosing the Precambrian "soda oceans" using Mg isotopes.

Declaration of Competing Interest

The authors declare that they have no known competing financial interests or personal relationships that could have appeared to influence the work reported in this paper.

Acknowledgments

We thank Shuang Yan for the help with the illustration in the

manuscript. The authors greatly appreciate the handling of the editor Michael E. Böttcher and the constructive comments of two anonymous reviewers that substantially enhanced this paper. This work is financially supported by the National Natural Science Foundation of China (Nos. 41973008, 41890845, 42073019 and 41621003), the "111" project (No. D17013), the Strategic Priority Research Program of Chinese Academy of Sciences (No. XDB26000000), and Key Laboratory of Ocean and Marginal Sea Geology, Chinese Academy of Sciences (No. OMG2020-02).

Appendix A. Supplementary data

Supplementary data to this article can be found online at https://doi.org/10.1016/j.chemgeo.2021.120565.

References

Akao, M., Marumo, F., Iwai, S., 1974. The crystal structure of hydromagnesite. Acta Crystallogr. B 30 (11), 2670–2672.
An, Z.-S., Colman, S.M., Zhou, W.-J., Li, X.-Q., Brown, E.T., Jull, A.J.T., Cai, Y.-J., Huang, Y.-S., Lu, X.-F., Chang, H., Song, Y.-G., Sun, Y.-B., Xu, H., Liu, W.-G., Jin, Z.-D., Liu, X.-D., Cheng, P., Liu, Y., Ai, L., Li, X.-Z., Liu, X.-J., Yan, L., Shi, Z.-G., Wang, X.-L., Wu, F., Qiang, X.-K., Dong, J.-B., Lu, F.-Y., Xu, X.-W., 2012. Interplay between the Westerlies and Asian monsoon recorded in Lake Qinghai sediments since 32 ka. Sci. Rep. 2 (619), 1–7.
Bąbel, M., Schreiber, B.C., 2014. Geochemistry of evaporites and evolution of seawater. In: Treatise on Geochemistry. Elsevier, Oxford, pp. 483–560.
Bao, Z., Huang, K.-J., Huang, T.-Z., Shen, B., Zong, C.-L., Chen, K.-Y., Yuan, H.-L., 2019. Precise magnesium isotope analyses of high-K and low-Mg rocks by MC-ICP-MS. J. Anal. At. Spectrom. 34 (5), 940–953.
Bao, Z., Huang, K.-J., Xu, J., Deng, L., Yang, S.-F., Zhang, P., Yuan, H.-L., 2020. Preparation and characterization of a new reference standard GSB-Mg for Mg isotopic analysis. J. Anal. At. Spectrom. 35, 1080–1086.
Bau, M., Dulski, P., 1996. Distribution of yttrium and rare-earth elements in the Penge and Kuruman iron-formations, Transvaal Supergroup, South Africa. Precambrian Res. 79, 37–55.
Blättler, C.L., Higgins, J.A., 2014. Calcium isotopes in evaporites record variations in Phanerozoic seawater SO_4 and Ca. Geology 42 (8), 711–714.
Blättler, C.L., Kump, L.R., Fischer, W.W., Paris, G., Kasbohm, J.J., Higgins, J.A., 2016. Constraints on ocean carbonate chemistry and P_{CO2} in the Archaean and Palaeoproterozoic. Nat. Geosci. 10 (1), 41–45.
Cangemi, M., Censi, P., Reimer, A., D'Alessandro, W., Hause-Reitner, D., Madonia, P., Oliveri, Y., Pecoraino, G., Reitner, J., 2016. Carbonate precipitation in the alkaline lake Specchio di Venere (Pantelleria Island, Italy) and the possible role of microbial mats. Appl. Geochem. 67, 168–176.
Cui, B.-L., Li, X.-Y., Wei, X.-H., 2016. Isotope and hydrochemistry reveal evolutionary processes of lake water in Qinghai Lake. J. Gt. Lakes Res. 42 (3), 580–587.
Dong, A., Zhu, X.-K., Li, S.Z., Kendall, B., Wang, Y., Gao, Z., 2016. Genesis of a giant Paleoproterozoic strata-bound magnesite deposit: constraints from Mg isotopes. Precambrian Res. 281, 673–683.
Feng, C.-Q., Gao, C.-H., Yin, Q.-Z., Jacobsen, B., Renne, P.R., Wang, J., Chang, S.-C., 2018. Tracking physicochemical conditions of evaporite deposition by stable magnesium isotopes: a case study of Late Permian Langbeinites. Geochem. Geophys. Geosyst. 19 (8), 2615–2630.
Frank, T.D., Fielding, C.R., 2003. Marine origin for Precambrian, carbonate-hosted magnesite? Geology 31 (12), 1101–1104.
Grotzinger, J.P., Kasting, J.F., 1993. New constraints on Precambrian ocean composition. J. Geol. 101 (2), 235–243.
Hardie, L.A., 1996. Secular variation in seawater chemistry: an explanation for the coupled secular variation in the mineralogies of marine limestones and potash evaporites over the past 600 m.y. Geology 24 (3), 279–283.
Harrison, A.L., Bénézeth, P., Schott, J., Oelkers, E.H., Mavromatis, V., 2021. Magnesium and carbon isotope fractionation during hydrated Mg-carbonate mineral phase transformations. Geochim. Cosmochim. Acta 293, 507–524.
Hawthorne, F.C., 1985. Refinement of the crystal structure of bloedite: structural similarities in the $[^{VI}M(^{IV}T\Phi_4)_2\Phi_n]$ finite-cluster minerals. Can. Mineral. 23 (4), 669–674.
Horita, J., Zimmermann, H., Holland, H.D., 2002. Chemical evolution of seawater during the Phanerozoic: Implications from the record of marine evaporites. Geochim. Cosmochim. Acta 66 (21), 3733–3756.
Jin, Z.-D., Wang, S.-M., Zhang, F., Shi, Y.-W., 2010. Weathering, Sr fluxes, and controls on water chemistry in the Lake Qinghai catchment, NE Tibetan Plateau. Earth Surf. Process. Landf. 35 (9), 1057–1070.
Kadoya, S., Krissansen-Totton, J., Catling, D.C., 2020. Probable cold and alkaline surface environment of the hadean earth caused by impact ejecta weathering. Geochem. Geophys. Geosyst. 21 e2019GC008734.
Kasting, J.F., Catling, D.C., 2003. Evolution of a habitable planet. Annu. Rev. Astron. Astrophys. 41, 429–463.
Kempe, S., Degens, E.T., 1985. An early soda ocean? Chem. Geol. 53 (1), 95–108.
Kempe, S., Kazmierczak, J., 1994. The role of alkalinity in the evolution of ocean chemistry, organization of living systems and biocalcification processes. Bull. Inst. Océanogr. Monaco 61–117.
Kempe, S., Kazmierczak, J., 2011. Soda Ocean Hypothesis, Encyclopedia of Geobiology. Springer Netherlands, Dordrecht, pp. 829–833.
Li, X.-Y., Xu, H.-Y., Sun, Y.-L., Zhang, D.-S., Yang, Z.-P., 2007. Lake-level change and water balance analysis at Lake Qinghai, West China during recent decades. Water Resour. Manag. 21 (9), 1505–1516.
Li, W., Beard, B.L., Johnson, C.M., 2011. Exchange and fractionation of Mg isotopes between epsomite and saturated $MgSO_4$ solution. Geochim. Cosmochim. Acta 75 (7), 1814–1828.
Li, W., Chakraborty, S., Beard, B.L., Romanek, C.S., Johnson, C.M., 2012. Magnesium isotope fractionation during precipitation of inorganic calcite under laboratory conditions. Earth Planet. Sci. Lett. 333–334, 304–316.
Ling, M.-X., Sedaghatpour, F., Teng, F.-Z., Hays, P.D., Strauss, J., Sun, W.-D., 2011. Homogeneous magnesium isotopic composition of seawater: an excellent geostandard for Mg isotope analysis. Rapid Commun. Mass Spectrom. 25 (19), 2828–2836.
Lowe, D.R., Worrell, G.F., 1999. Sedimentology, mineralogy, and implications of silicified evaporites in the Kromberg Formation, Barberton Greenstone Belt, South Africa. In: Geological Society of America Special Paper, 329, pp. 167–188.
Lyons, T.W., Reinhard, C.T., Planavsky, N.J., 2014. The rise of oxygen in Earth's early ocean and atmosphere. Nature 506, 307–315.
Mavromatis, V., Pearce, C.R., Shirokova, L.S., Bundeleva, I.A., Pokrovsky, O.S., Benezeth, P., Oelkers, E.H., 2012. Magnesium isotope fractionation during hydrous magnesium carbonate precipitation with and without cyanobacteria. Geochim. Cosmochim. Acta 76, 161–174.
Mavromatis, V., Gautier, Q., Bosc, O., Schott, J., 2013. Kinetics of Mg partition and Mg stable isotope fractionation during its incorporation in calcite. Geochim. Cosmochim. Acta 114, 188–203.
Mavromatis, V., Power, I.M., Harrison, A.L., Beinlich, A., Dipple, G.M., Bénézeth, P., 2021. Mechanisms controlling the Mg isotope composition of hydromagnesite-magnesite playas near Atlin, British Columbia, Canada. Chem. Geol. 579, 120325.
McCaffrey, M.A., Lazar, B., Holland, H.D., 1987. The evaporation path of seawater and the coprecipitation of Br^- and K^+ with halite. Geochim. Cosmochim. Acta 57 (5), 928–937.
Nielsen, L.C., DePaolo, D.J., 2013. Ca isotope fractionation in a high-alkalinity lake system: Mono Lake, California. Geochim. Cosmochim. Acta 118, 276–294.
Oelkers, E.H., Berninger, U.-N., Pérez-Fernàndez, A., Chmeleff, J., Mavromatis, V., 2018. The temporal evolution of magnesium isotope fractionation during hydromagnesite dissolution, precipitation, and at equilibrium. Geochim. Cosmochim. Acta 226, 36–49.
Parkhurst, D.L., Appelo, C.A.J., 2013. Description of Input and Examples for PHREEQC Version 3-a computer program for speciation, batch-reaction, one-dimensional transport, and inverse geochemical calculations. In: U.S. Geol. Surv. Tech. Methods, B. 6, Chapter A43, 6−43A.
Pearce, C.R., Saldi, G.D., Schott, J., Oelkers, E.H., 2012. Isotopic fractionation during congruent dissolution, precipitation and at equilibrium: evidence from Mg isotopes. Geochim. Cosmochim. Acta 92, 170–183.
Power, I., Wilson, S., Thom, J., Dipple, G., Southam, G., 2007. Biologically induced mineralization of dypingite by cyanobacteria from an alkaline wetland near Atlin, British Columbia, Canada. Geochem. Trans. 8 (1), 1–16.
Power, I.M., Harrison, A.L., Dipple, G.M., Wilson, S.A., Barker, S.L.L., Fallon, S.J., 2019. Magnesite formation in playa environments near Atlin, British Columbia. Canada. Geochim. Cosmochim. Acta 255, 1–24.
Sanz-Montero, M.E., Cabestrero, Ó., Sánchez-Román, M., 2019. Microbial Mg-rich carbonates in an extreme alkaline lake (Las Eras, Central Spain). Front. Microbiol. 10 (148), 1–15.
Schauble, E.A., 2011. First-principles estimates of equilibrium magnesium isotope fractionation in silicate, oxide, carbonate and hexaaquamagnesium($^{2+}$) crystals. Geochim. Cosmochim. Acta 75 (3), 844–869.
Shalev, N., Lazar, B., Köbberich, M., Halicz, L., Gavrieli, I., 2018. The chemical evolution of brine and Mg-K-salts along the course of extreme evaporation of seawater – an experimental study. Geochim. Cosmochim. Acta 241, 164–179.
Shalev, N., Lazar, B., Halicz, L., Gavrieli, I., 2021. The Mg isotope signature of marine Mg-evaporites. Geochim. Cosmochim. Acta 301, 30–47.
Shirokova, L.S., Mavromatis, V., Bundeleva, I.A., Pokrovsky, O.S., Bénézeth, P., Gérard, E., Pearce, C.R., Oelkers, E.H., 2013. Using Mg isotopes to trace cyanobacterially mediated magnesium carbonate precipitation in alkaline lakes. Aquat. Geochem. 19 (1), 1–24.
Stanley, S.M., Hardie, L.A., 1998. Secular oscillations in the carbonate mineralogy of reef-building and sediment-producing organisms driven by tectonically forced shifts in seawater chemistry. Palaeogeogr. Palaeoclimatol. Palaeoecol. 144 (1), 3–19.
Stüeken, E.E., Buick, R., Schauer, A.J., 2015. Nitrogen isotope evidence for alkaline lakes on late Archean continents. Earth Planet. Sci. Lett. 411, 1–10.
Sugitani, K., Mimura, K., Suzuki, K., Nagamine, K., Sugisaki, R., 2003. Stratigraphy and sedimentary petrology of an Archean volcanic–sedimentary succession at Mt. Goldsworthy in the Pilbara Block, Western Australia: implications of evaporite (nahcolite) and barite deposition. Precambrian Res. 120 (1), 55–79.
Sun, D.-P., Li, B.-X., Ma, Y.-H., Liu, Q.-Z., 1995. An investigation on evaporating experiments for Qinghai-Lake water, China. J. Sal. La. Sci. 3 (2), 10–19.
Sun, D.-P., Li, B.-X., Ma, Y.-H., Liu, Q.-Z., 2002. An investigation on evaporating experiments for Qinghai Lake water, China. J. Sal. La. Res. 10 (4), 1–12.
Thompson, J.B., Ferris, F.G., 1990. Cyanobacterial precipitation of gypsum, calcite, and magnesite from natural alkaline lake water. Geology 18 (10), 995–998.

Tucker, M.E., 1982. Precambrian dolomites: petrographic and isotopic evidence that they differ from Phanerozoic dolomites. Geology 10 (1), 7–12.
Vengosh, A., Starinsky, A., Kolodny, Y., Chivas, A.R., Raab, M., 1992. Boron isotope variations during fractional evaporation of sea water: new constraints on the marine vs. nonmarine debate. Geology 20 (9), 799–802.
Warren, J.K., 2010. Evaporites through time: tectonic, climatic and eustatic controls in marine and nonmarine deposits. Earth Sci. Rev. 98 (3), 217–268.
Warren, J.K., 2016. Evaporites. In: Encyclopedia of Geochemistry. Springer, Dordrecht, pp. 1–8.
Xia, Z., Horita, J., Reuning, L., Bialik, Or M., Hu, Z., Waldmann, N.D., Liu, C., Li, W., 2020. Extracting Mg isotope signatures of ancient seawater from marine halite: a reconnaissance. Chem. Geol. 552, 119768.